Differential Coupling through Val-344 and Tyr-442 of Trimethylamine Dehydrogenase in Electron Transfer Reactions with Ferricenium Ions and Electron Transferring Flavoprotein†

Jaswir Basran,‡ Kamaldeep K. Chohan,§ Michael J. Sutcliffe,§ and Nigel S. Scrutton*,‡

Department of Biochemistry, University of Leicester, University Road, Leicester LE1 7RH, U.K., and Department of Chemistry, University of Leicester, University Road, Leicester LE1 7RH, U.K.

Received March 27, 2000; Revised Manuscript Received May 5, 2000

ABSTRACT: Modeling studies of the trimethylamine dehydrogenase−electron transferring flavoprotein (TMADH−ETF) electron transfer complex have suggested potential roles for Val-344 and Tyr-442, found on the surface of TMADH, in electronic coupling between the 4Fe−4S center of TMADH and the FAD of ETF. The importance of these residues in electron transfer, both to ETF and to the artificial electron acceptor, ferricenium (Fc^+), has been studied by site-directed mutagenesis and stopped-flow spectroscopy. Reduction of the 6-(*S*)-cysteinyl FMN in TMADH is not affected by mutation of either Tyr-442 or Val-344 to a variety of alternate side chains, although there are modest changes in the rate of internal electron transfer from the 6-(*S*)-cysteinyl FMN to the 4Fe−4S center. The kinetics of electron transfer from the 4Fe−4S center to Fc^+ are sensitive to mutations at position 344. The introduction of smaller side chains (Ala-344, Cys-344, and Gly-344) leads to enhanced rates of electron transfer, and likely reflects shortened electron transfer "pathways" from the 4Fe−4S center to Fc^+. The introduction of larger side chains (Ile-344 and Tyr-344) reduces substantially the rate of electron transfer to Fc^+. Electron transfer to ETF is not affected, to any large extent, by mutation of Val-344. In contrast, mutation of Tyr-442 to Phe, Leu, Cys, and Gly leads to major reductions in the rate of electron transfer to ETF, but not to Fc^+. The data indicate that electron transfer to Fc^+ is via the shortest pathway from the 4Fe−4S center of TMADH to the surface of the enzyme. Val-344 is located at the end of this pathway at the bottom of a small groove on the surface of TMADH, and Fc^+ can penetrate this groove to facilitate good electronic coupling with the 4Fe−4S center. With ETF as an electron acceptor, the observed rate of electron transfer is substantially reduced on mutation of Tyr-442, but not Val-344. We conclude that the flavin of ETF does not penetrate fully the groove on the surface of TMADH, and that electron transfer from the 4Fe−4S center to ETF may involve a longer pathway involving Tyr-442. Mutation of Tyr-442 likely disrupts electron transfer by perturbing the interaction geometry of TMADH and ETF in the productive electron transfer complex, leading to less efficient coupling between the redox centers.

Trimethylamine dehydrogenase (TMADH,[1] EC 1.5.99.7) is an iron−sulfur flavoprotein that catalyzes the oxidative demethylation of trimethylamine (TMA) to dimethylamine (DMA) and formaldehyde (*1*):

$$(CH_3)_3N + H_2O \rightarrow (CH_3)_2NH + CH_2O + 2H^+ + 2e^-$$

The enzyme is isolated from the bacterium *Methylophilus methylotrophus* (sp. W_3A_1) and is homodimeric. Each subunit has a molecular mass of 83 kDa and contains a covalently linked 6-(*S*)-cysteinyl FMN and a ferredoxin type 4Fe−4S center (*1*−*6*). ADP is also bound by each subunit, but a role for this nucleotide in catalysis has not been demonstrated (*7*). The physiological electron acceptor of TMADH is an electron transferring flavoprotein (ETF) (*8*). ETF is heterodimeric and contains 1 equiv of FAD (*8*) and AMP (*9*) per heterodimer. ETF cycles between oxidized and (anionic) semiquinone oxidation states (*8*), although two-electron reduction of ETF can be achieved electrochemically (*10*) or when it is in complex with TMADH (*11*). Models of ETF, based on the crystal structure of the homologous human protein, suggest the protein is highly dynamic (*12*, *13*). In free solution, ETF populates many conformations, with domain II pivoting around two hinge sequences that connect this domain to domains I and III of the molecule (*14*). To enable its interaction with TMADH, domain II of ETF is required to interact with domain III, thus enabling ETF to dock at a concave interaction site on the surface of TMADH (*12*). Complex assembly thus involves an "induced fit" mechanism for this transient protein−protein interaction.

† This work was funded by grants from the Biotechnology and Biological Sciences Research Council, the Royal Society, and the Lister Institute of Preventive Medicine. N.S.S. is a Lister Institute Research Fellow.

* To whom correspondence should be addressed: Department of Biochemistry, University of Leicester, University Road, Leicester LE1 7RH, U.K. Telephone: +44 116 223 1337. Fax: +44 116 252 3369. E-mail: nss4@le.ac.uk.

‡ Department of Biochemistry, University of Leicester.

§ Department of Chemistry, University of Leicester.

[1] Abbreviations: TMADH, trimethylamine dehydrogenase; ETF, electron transferring flavoprotein; Fc^+, ferricenium ion.

10.1021/bi0006868 CCC: $19.00
Published on Web 07/11/2000

The reductive half-reaction of TMADH proceeds in three kinetically resolvable phases (*15*−*21*). The fast phase represents two-electron reduction of the 6-(*S*)-cysteinyl FMN cofactor (or, alternatively, formation of a covalent substrate−flavin adduct possessing an absorption spectrum similar to that of reduced flavin) following cleavage of a C−H bond in one of the substrate methyl groups. The mode by which the bond is broken is unknown, but has recently been debated in the context of detailed kinetic studies (*21*). The intermediate kinetic phase reports on intramolecular electron transfer from reduced flavin to the 4Fe−4S center. Internal electron transfer over this short distance [approximately 4 Å from the 8α-methyl group of the flavin to the nearest cysteinyl ligand of the 4Fe−4S center (*22*)] is slow, and this may reflect the breakdown of a flavin−substrate adduct in the fast phase of the reaction. Internal electron transfer from the flavin to the 4Fe−4S center generates the flavin semiquinone and the reduced 4Fe−4S center. The slow phase of the reductive half-reaction involves dissociation of the product and binding of a second substrate molecule, which perturbs the electronic distribution in partially reduced enzyme to facilitate formation of the so-called spin-interacting state. In this state, the unpaired spins in the flavin semiquinone and reduced 4Fe−4S center become ferromagnetically coupled and give rise to an unusual EPR signal, centered near $g \sim 2$, and an unusual half-field $g \sim 4$ signal (*15*−*19*). Electronic redistribution in the flavin and formation of the spin-interacting state is the result of substrate-induced ionization of Tyr-169, which is located close to the pyrimidine ring of the 6-(*S*)-cysteinyl FMN (*23*).

The transfer of electrons from TMADH to ETF (the oxidative half-reaction) has been studied by stopped-flow methods (*24*). Reaction of two-electron reduced TMADH with oxidized ETF gives rise to complex multiphasic kinetics (*24*). Studies of the oxidative half-reaction have been simplified; inactivation of the 6-(*S*)-cysteinyl FMN by treatment with phenylhydrazine places a phenyl group on the C4a atom of the flavin, rendering it redox inert (*24*, *25*). Enzyme treated in this way can be reduced (under anaerobic conditions) to the level of one reducing equivalent by titration with dithionite; the electron is located in the 4Fe−4S center. Rapid mixing of one-electron-reduced TMADH with oxidized ETF gives rise to biphasic kinetic transients. The fast phase of these transients reports on interprotein electron transfer and is dependent on ETF concentration; the origin of the slow phase is as yet uncertain (*24*). Reactions have been performed with three-electron-reduced TMADH and ETF. In this case, the fast phase of the transient obtained is similar in rate to the fast phase of the biphasic transient obtained with phenylhydrazine-inactivated TMADH, confirming this phase reports on electron transfer from the 4Fe−4S center to ETF. A dissociation constant of about 3−7 μM has been measured by quantitative sedimentation equilibrium methods in the analytical ultracentrifuge for complexes of oxidized TMADH and semiquinone ETF (*26*). In this paper, we have assessed the importance of residues Tyr-442 and Val-344 of TMADH in electron transfer to ETF and an artificial electron acceptor, Fc^+.

EXPERIMENTAL PROCEDURES

Mutagenesis of TMADH. The Y442F, Y442L, and Y442G TMADH mutants were constructed as described elsewhere (*27*). Mutations at position 344 in TMADH (V344G, V344C, V344A, V344I, and V344Y) and the Y442C mutant TMADH were made using the QuikChange Site Directed Mutagenesis kit supplied by Stratagene. Putative mutants were sequenced by dideoxynucleotide sequencing using the Pharmacia T7 sequencing kit and protocols. Each mutant gene was completely resequenced to ensure that no spurious changes had arisen as a result of the mutagenesis procedure. Mutant enzymes were expressed in *Escherichia coli* under the control of the *Bacillus subtilis* vegetative promoter as described previously (*28*).

Purification of TMADH and ETF. Native TMADH isolated from *M. methylotrophus* (sp. W_3A_1) was purified as described previously (*1*). Recombinant native and mutant forms of TMADH were purified also as described previously (*28*), but with some modifications (*29*). As seen with other mutant forms of TMADH (*28*), the recombinant native and mutant TMADH enzymes contained the full complement of a 4Fe−4S center and ADP, but the level of flavinylation varied from 20 to 35%. Partial flavinylation is known not to affect the kinetic behavior of TMADH. The flavin content and extinction coefficient for each TMADH mutant was determined spectrophotometrically as outlined previously (*28*). The concentration of the native enzyme was calculated using the molar extinction coefficient for the oxidized enzyme [$\epsilon_{443} = 27\,300\ M^{-1}\ cm^{-1}$ (*6*)].

ETF was purified from *M. methylotrophus* (sp. W_3A_1) as described previously (*8*). The protein, which is purified as a mixture of oxidized and reduced (anionic semiquinone) forms (*8*), was oxidized completely by treatment with potassium ferricyanide, followed by gel filtration to remove excess oxidant. The concentration of oxidized ETF was determined spectrophotometrically at 438 nm [$\epsilon_{438} = 11\,300\ M^{-1}\ cm^{-1}$ (*8*)].

Treatment of TMADH with Phenylhydrazine Hydrochloride. Phenylation of the 6-(*S*)-cysteinyl FMN of TMADH was achieved by treatment with phenylhydrazine (*6*, *25*). TMADH (50 μM), contained in 100 mM sodium pyrophosphate buffer (pH 7.7), was incubated with 2 mM phenylhydrazine, 1 mM PMS, and 70 μM DCPIP at 30 °C for 3 h. The sample was then passed through a small gel filtration column to remove the excess phenylhydrazine and electron acceptors. The concentration of phenylhydrazine-inactivated TMADH was determined at 280 nm ($\epsilon_{280} = 201\,610\ M^{-1}\ cm^{-1}$).

Preparation of Anaerobic Samples and Reduction of TMADH with Dithionite. Solutions of anaerobic 50 mM potassium phosphate (pH 7.0) were made by bubbling nitrogen gas through the solutions for 2 h. Solutions were then placed in an anaerobic glovebox (Belle Technology) overnight to remove residual traces of oxygen. Protein samples were made anaerobic by passing them through a small gel filtration column that had been pre-equilibrated in anaerobic buffer and housed in the glovebox. Solutions of sodium dithionite were made by adding solid sodium dithionite to anaerobic buffer. TMADH was reduced to the level of one electron (reduction of the 4Fe−4S center in the phenylhydrazine-inactivated enzyme) or three electrons (reduction of both redox centers in native TMADH) by titration with sodium dithionite. Microliter volumes of a stock sodium dithionite solution were added to the anaerobic enzyme sample, and reduction was followed by monitoring

the absorbance changes of the protein from 300 to 600 nm.

Steady-State Kinetic Assays. Steady-state kinetic measurements using either ETF or Fc^+ as the electron acceptor were performed at 25 °C using a Hewlett-Packard 8452A single-beam diode array spectrophotometer. The reaction mixture contained 50 mM potassium phosphate buffer (pH 7.0), 100 μM trimethylamine, and a fixed concentration of native or mutant TMADH; the reaction was initiated by the addition of the electron acceptor. When ETF was used as the oxidant, the reaction was monitored at 370 nm using the difference molar extinction coefficient of 7830 M^{-1} cm^{-1} between the oxidized and anionic semiquinone forms of the protein (*8*). The reduction of Fc^+ was monitored at 300 nm using a difference extinction coefficient of 4300 M^{-1} cm^{-1} (*30*). Data were fitted using the Grafit software package (*31*) to either the Michaelis−Menten equation or, when inhibition was observed, eq 1 (*32*).

$$v = \frac{\left(1 + \frac{b[S]}{K_i}\right)V_{max}}{1 + \frac{K_s}{[S]} + \frac{K_s}{K_i} + \frac{[S]}{K_i}} \quad (1)$$

Single-Turnover Stopped-Flow Kinetic Experiments. Rapid reaction studies were performed using an Applied Photophysics SX.17MV stopped-flow spectrometer housed within a customized glovebox (Belle Technology Ltd.) or using an Applied Photophysics SX.18MV stopped-flow instrument. All reactions were carried out in 50 mM potassium phosphate buffer (pH 7.0) at the stated temperatures. To ensure pseudo-first-order conditions in single-turnover experiments, the concentrations of the substrate (in the reductive half-reaction experiments) and of the electron acceptor (in the oxidative half-reaction experiments) were at least 10- and 5-fold greater than that of TMADH, respectively. For each substrate or electron acceptor concentration, at least five replicate measurements were collected and averaged. Data were analyzed using nonlinear least-squares regression analysis on an Acorn RISC PC microcomputer using Spectrakinetics software (Applied Photophysics).

Analysis of the reductive half-reaction kinetics was carried out at 20 °C as described previously (*21*). Reduction of the flavin by substrate was observed by following the absorbance change at 443 nm. Internal electron transfer from the flavin to the 4Fe−4S center was observed at 365 nm by following the biphasic absorbance change associated with formation of the flavin anionic semiquinone and the so-called spin-interacting state of TMADH (*21*). Reaction scheme modeling and evaluation of rate constants by nonlinear least-squares fitting was as described previously for native TMADH (*21*). Substrate-reduced TMADH is quite stable to reoxidation by air [half-life $\sim$ 50 min (*29*)], which negated the use of anaerobic conditions when carrying out the reductive half-reaction experiments.

When the rate of electron transfer from dithionite-reduced TMADH to either the physiological electron acceptor ETF or the artificial electron acceptor Fc^+ (in the form of ferricenium hexafluorophosphate) was measured, experiments were carried out anaerobically. This was achieved by housing the sample handling unit of the stopped-flow instrument within an anaerobic glovebox (*33*). In studies of the oxidative half-reaction, the concentration of TMADH was fixed (3.5 μM) and was mixed with an equal volume of oxidant. Reoxidation of phenylhydrazine-treated, dithionite-reduced TMADH by ETF was monitored at a wavelength of 370 nm and at 5 °C as described for the native enzyme (*24*); reoxidation of dithionite-reduced TMADH by Fc^+ was followed at 440 nm and at 25 °C. Transients obtained for the reoxidation of TMADH using either electron acceptor were biphasic, and the rate constants for both phases (k_{fast} and k_{slow}) were obtained by fitting the data to a double-exponential expression. In these experiments, k_{fast} represents the rate of electron transfer from TMADH to the electron acceptor and was plotted as a function of the electron acceptor concentration. Details of reaction scheme modeling are given in the Results and Discussion.

Complex Formation (TMADH−Fc^+) and Calculation of Intrinsic Electron Transfer Rate Constants. The three-dimensional crystal structure of TMADH (1.7 Å resolution; F. S. Mathews et al., unpublished) from the bacterium *M. methylotrophus* (sp. W_3A_1) was used in conjunction with the Cartesian coordinates of Fc^+, obtained from the Cambridge Crystallographic Database (*34*). The program Dock (*35*) was used to produce models of the TMADH−Fc^+ complex. For input into Dock, both TMADH and Fc^+ were charged within the program Sybyl (Tripos Inc., St. Louis, MO). A maximum of 500 orientations of Fc^+ (with respect to TMADH) were sampled by Dock, and the 10 highest-ranked Fc^+ dockings (based on energy) were obtained, thus giving 10 TMADH−Fc^+ complexes. The intrinsic rate constant, k_{eT}, for transfer from the 4Fe−4S center of TMADH to the Fc^+ was calculated for the highest-ranked Fc^+ docking using the program ET_Rates (*36*), which uses the empirical expression for exergonic electron tunneling:

$$\log_{10} k_{eT} = 13.0 - (1.2 - 0.8\rho)(R - 3.6) - 3.1(\Delta G + \lambda)^2/\lambda \quad (2)$$

where ρ is the fraction of the volume between redox cofactors that is within the united van der Waals radius of intervening atoms. Two approaches were used for calculating k_{eT}: (i) electron transfer from the 4Fe−4S center to the Fc^+ as a whole and (ii) electron transfer from the 4Fe−4S center to the Fe atom of the Fc^+. The k_{eT} obtained was corrected for the Gibbs free energy, ΔG (−0.28 eV; calculated from the known potentials of the 4Fe−4S center and Fc^+), and the reorganization energy,[2] λ {0.7 eV; i.e., $[-3.1(\Delta G + \lambda)^2/\lambda] = -0.79$ eV for transfer from the 4Fe−4S center to Fc^+}. The docking and electron transfer calculations were repeated for the following TMADH mutants: V344A, V344C, V344G, V344I, V344Y, Y442F, Y442L, Y442C, and Y442G. Mutants were generated, on the basis of the native TMADH crystal structure, using the program Insight II (MSI, San Diego, CA).

RESULTS

Potential Electron Transfer Pathways from the 4Fe−4S Center to the Surface of TMADH. The crystal structure of TMADH has been determined at 1.7 Å resolution. Although

[2] The value of λ is taken from the work of Dutton and colleagues (*36*), and represents a typical value for the reorganizational energy for biological electron transfer reactions.

Table 1: Steady-State Kinetic Parameters for Mutants of TMADH Altered at Positions V344 and Y442 with ETF as the Electron Acceptor[a]

enzyme	K_m (μM)	k_{cat} (s^{-1})
native TMADH	14.8 ± 1.2	16.8 ± 0.5
V344A	22.0 ± 2.5	10.0 ± 0.4
V344C	15.1 ± 1.3	11.5 ± 0.3
V344G	18.1 ± 1.2	9.1 ± 0.2
V344I	24.2 ± 2.6	6.7 ± 0.3
V344Y	24.0 ± 1.4	8.6 ± 0.2
Y442F	19.1 ± 0.6	9.0 ± 0.1
Y442L	21.8 ± 2.8	4.2 ± 0.2
Y442C	24.0 ± 1.6	0.9 ± 0.02
Y442G	65.9 ± 11	0.5 ± 0.05

[a] Reaction conditions: 50 mM phosphate buffer at pH 7.0 and 25 °C.

structures for human ETF (*13*) and ETF from *Paracoccus denitrificans* (*37*) have been determined, no structure is known for *M. methylophilus* ETF. In previous work, we produced a homology model of *M. methylophilus* ETF (using the crystallographic coordinates for human ETF) and a model of the complex formed between TMADH and ETF (*12*). This modeling work, coupled with kinetic studies of three mutant forms of TMADH altered at residue Tyr-442, revealed the existence of a small surface groove on TMADH that may accommodate the isoalloxazine ring of the FAD bound to ETF. Our earlier modeling studies, together with an analysis of the major electron transfer pathways using the PATHWAYS II algorithm (which invokes heterogeneity in the protein bridge (*38*); for the current study, we have used instead an approach which treats the protein bridge as homogeneous, and the reasons for this are discussed at the end of the Results), revealed two major potential routes for electron transfer from the 4Fe−4S center of TMADH to the FAD of ETF. The first pathway is the shortest and extends from Cys-345 (a ligand of the 4Fe−4S center) to Val-344; Val-344 is located at the bottom of a small groove found on the surface of TMADH. The second pathway extends from Cys-345 to Glu-439 and then to residue Tyr-442; this latter residue forms one side of the groove on the surface of the enzyme (see Figure 6). Previous mutagenesis studies revealed the importance of Tyr-442 in electron transfer to ETF (*27*). The purpose of this work is to assess the relative contributions made by Val-344 and Tyr-442 in electron transfer to ETF, and also to artificial acceptors such as Fc^+. The aim is to provide a more focused appraisal of the role of these residues in the oxidative half-reaction of TMADH. To this end, we isolated five mutant enzymes altered at position 344; three were designed to reduce (Cys-344, Ala-344, and Gly-344) and two to increase (Ile-344 and Tyr-344) the side chain volume at this location. We have also extended our previous analysis of three mutants altered at position 442 (Phe-442, Leu-442, and Gly-442) and have included studies of a new mutant at this position (Cys-442).

Steady-State Kinetic Experiments. Steady-state kinetic parameters for the native and mutant enzymes with ETF as the electron acceptor are shown in Table 1. Reaction rates were measured at a TMA concentration of 100 μM to minimize the effect of substrate inhibition that is known to occur at higher substrate concentrations (*32*). Consequently, all kinetic parameters that are reported are apparent values. In all cases, simple Michaelis−Menten kinetic behavior was

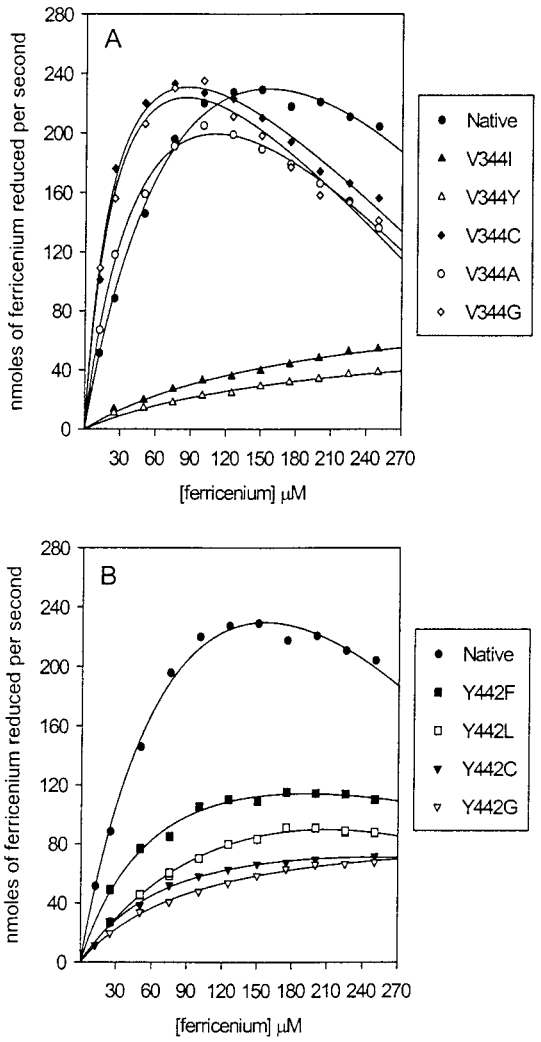

FIGURE 1: Steady-state kinetic analysis of the reaction of native and mutant TMADH enzymes with the artificial electron acceptor Fc^+. (A) Plot of velocity vs $[Fc^+]$ for the native and V344 mutant TMADH enzymes. (B) Plot of velocity vs $[Fc^+]$ for the native and Y442 mutant TMADH enzymes. Reaction conditions: 50 mM potassium phosphate buffer at pH 7 and 25 °C. The kinetic parameters are displayed in Table 2.

observed (range of ETF concentrations of 0−90 μM). The Michaelis constant, K_m, remains largely unaffected by substitutions at positions Val-344 and Tyr-442 in TMADH, although there is a modest (5-fold) increase for the Y442G mutant. The effect on k_{cat} was also minimal for the Val-344 mutants (an at most 2-fold decrease for V344I TMADH compared to that of the native enzyme). However, the Tyr-442 substitutions did have a more noticeable effect, with the smaller and less bulky Cys and Gly replacements leading to a 19- and 31-fold reduction in turnover number, respectively, compared to that of the native enzyme.

Plots of the reaction rate against Fc^+ concentration for the native and mutant enzymes are shown in Figure 1, and the steady-state kinetic parameters are listed in Table 2. For the native enzyme and the majority of TMADH mutants that were studied (with the exceptions of V344I, V344Y, and Y442G), inhibition kinetics were observed at high Fc^+ concentrations. For enzymes that displayed inhibition, the kinetic parameters K_m and k_{cat} were obtained from fits of the data to eq 1 (*32*); for the V344I, V344Y, and Y442G mutants, these parameters were obtained by fitting the data

Table 2: Steady-State Kinetic Parameters for Mutants of TMADH Altered at Positions V344 and Y442 with Fc^+ as the Electron Acceptor[a]

enzyme	K_m (μM)	k_{cat} (s^{-1})	k_{cat}/K_m ($\times 10^6$ M^{-1} s^{-1})
native TMADH	140 ± 28	33.4 ± 4.7	0.24 ± 0.08
V344A	63.5 ± 6.2	22.3 ± 1.2	0.35 ± 0.05
V344C	28.5 ± 3.6	19.9 ± 1	0.70 ± 0.12
V344G	31.0 ± 4.9	20.1 ± 1.3	0.65 ± 0.14
V344I[b]	189 ± 24	4.8 ± 0.3	0.026 ± 0.005
	(48.4 ± 17)	(1.8 ± 0.4)	(0.037 ± 0.02)
V344Y[b]	195 ± 33	3.5 ± 0.3	0.018 ± 0.005
	(191 ± 15)	(3.4 ± 0.2)	(0.02 ± 0.003)
Y442F	87.5 ± 20	11.5 ± 1.7	0.13 ± 0.05
Y442L	323 ± 78	19.1 ± 4.0	0.06 ± 0.03
Y442C[b]	63.8 ± 6.2	4.8 ± 0.2	0.07 ± 0.01
	(100 ± 21)	(6.6 ± 1.0)	(0.07 ± 0.03)
Y442G[b]	96.7 ± 6.0	5.0 ± 0.1	0.05 ± 0.004
	(112 ± 28)	(5.5 ± 1.0)	(0.05 ± 0.02)

[a] Reaction conditions: 50 mM phosphate buffer at pH 7.0 and 25 °C. Kinetic parameters were calculated by fitting to eq 1, except where noted otherwise. [b] Kinetic parameters obtained by fitting to the Michaelis−Menten equation. Kinetic parameters shown in parentheses obtained by fitting to eq 1.

Table 3: Limiting Flavin Reduction Rates (k_{lim}), Enzyme−Substrate Dissociation Constants (K_d), and Rates of Internal Electron Transfer (k_{int}) for the Reaction of Native and Mutant TMADH Enzymes with TMA[a]

enzyme	K_d (mM) (443 nm, pH 7)	k_{lim} (s^{-1}) (443 nm, pH 7)	k_{int} (s^{-1}) (365 nm, pH 8)
native TMADH	11.5 ± 0.6	971 ± 43	40.1
V344A	8.75 ± 0.8	942 ± 34	55.2
V344C	12.0 ± 1.3	1024 ± 46	60.1
V344G	12.2 ± 1.8	997 ± 62	54.4
V344I	15.4 ± 2.3	1140 ± 78	53.7
V344Y	9.54 ± 1.4	936 ± 56	47.3
Y442F	8.31 ± 0.5	821 ± 19	30.0
Y422L	7.91 ± 1.0	849 ± 37	20.8
Y422C	7.50 ± 0.6	844 ± 25	32.6
Y422G	9.72 ± 0.9	899 ± 33	40.4

[a] The values of k_{lim} and K_d were calculated from hyperbolic plots of the observed rate of flavin reduction at 443 nm vs [TMA] at pH 7. The values of k_{int} were obtained from biphasic transients measured at 365 nm and pH 8 as described previously (*21*). k_{int} values are observed values measured at a [TMA] of 100 μM. Reaction conditions: 50 mM potassium phosphate buffer at pH 7 and 20 °C or 50 mM sodium pyrophosphate buffer at pH 8 and 20 °C.

to the standard hyperbolic expression. Mutations at position 344 in TMADH have quite dramatic effects on the steady-state kinetic behavior with Fc^+ (Table 2 and Figure 1). Substitution of Val-344 with Cys, Ala, or Gly leads to a reduction in the apparent K_m for Fc^+ and an increase in the reaction rate (k_{cat}/K_m) catalyzed by these mutants in the noninhibitory regime of the plot. However, there is only a modest (no more than 2-fold) effect on k_{cat} compared to that of the native enzyme. Recently, the mechanism of substrate inhibition in TMADH was elucidated (ref *32* and Discussion). The results obtained with the V344A, V344C, and V344G mutants (Figure 1) suggest that the partitioning between the two cycles is shifted in favor of the 1/3 cycle in the mutant proteins (in which electron transfer to Fc^+ is faster than in the native enzyme; see below). In contrast, the V344I and V344Y mutants do not show inhibition to any great extent under the conditions used in this study (Figure 1), and electron transfer to Fc^+ is slower compared with that to native TMADH (also see below). Clearly, the inhibition seen with the Fc^+ ion is more complex than with TMA, and these complexities are discussed in relation to the branching kinetic mechanism in the Discussion.

The Tyr-442 substitutions do not have any major effect on the steady-state kinetic behavior of TMADH with Fc^+. The apparent K_m value for all the Tyr-442 mutant enzymes is comparable to the native enzyme, and a maximal 6-fold reduction in turnover number is seen for the Y442G mutant compared to that of the native enzyme. Unlike those with the Val-344 mutants, the data suggest that mutations at position Tyr-442 have little effect on the kinetics of electron transfer to Fc^+. Detailed stopped-flow kinetic analyses of the oxidative half-reaction in each mutant form of the TMADH enzyme corroborate this assertion (see below).

Kinetics of the Reductive Half-Reaction. To assess if any of the mutations at position Val-344 or Tyr-442 affect the kinetics of the reductive half-reaction, the limiting rates of flavin reduction (substrate oxidation) and subsequent electron transfer to the 4Fe−4S center were measured under conditions similar to those of the oxidative half-reaction (Table 3 and Figure 2). In TMADH, both Val-344 and Tyr-442 are located at the center of a large concave region on the surface of the protein thought to form part of the docking site for ETF (*12*, *27*). Both residues are some distance from the 6-(*S*)-cysteinyl FMN, and as expected, the mutations were found to have little or no effect on the binding or limiting rate constant (k_{lim}) for oxidation of the substrate (Table 3).

Absorbance changes at 365 nm can be used to calculate the rate of intramolecular electron transfer from the 6-(*S*)-cysteinyl FMN to the 4Fe−4S center and the kinetics of formation of the spin-interacting state (*21*). For native TMADH, the kinetic transients are typically biphasic in nature with the fast phase of the absorbance change being associated with intramolecular electron transfer (k_{int}). This phase is followed by a second, slower phase (k_{slow}), which reflects product dissociation and formation of the spin-interacting state as a result of electronic redistribution in the flavin following binding of a second substrate molecule at the active site (*23*). However, the kinetics are complicated further by the fact that the extent of the biphasic nature changes as a function of both TMA concentration and pH (*21*). For example, at pH 7 (the value used in the study presented here), the majority of the absorbance change at 365 nm (approximately 90%) is attributed to the slow phase. Thus, the relatively small absorbance change associated with the fast phase means that k_{int} cannot be measured accurately at pH 7. Values for k_{slow} (pH 7) were measured for native and mutant TMADH enzymes over a range of TMA concentrations. Values for k_{int} [pH 8, where the contribution of the intermediate phase is increased (*21*)] were measured at a fixed TMA concentration of 100 μM (Table 3), although it is acknowledged that the rates also show a complex dependence on TMA concentration (*21*). The data for k_{slow} as a function of TMA concentration are shown in Figure 2, and the mutants display the same complex dependence on TMA concentration as seen previously for the native enzyme (*21*). However, small changes in rate are observed that may reflect minor structural perturbations around the 4Fe−4S center as a result of mutating residues Tyr-442 and Val-344, which are close to this redox center. The data presented in Table 3 indicate small perturbations in k_{int} throughout the

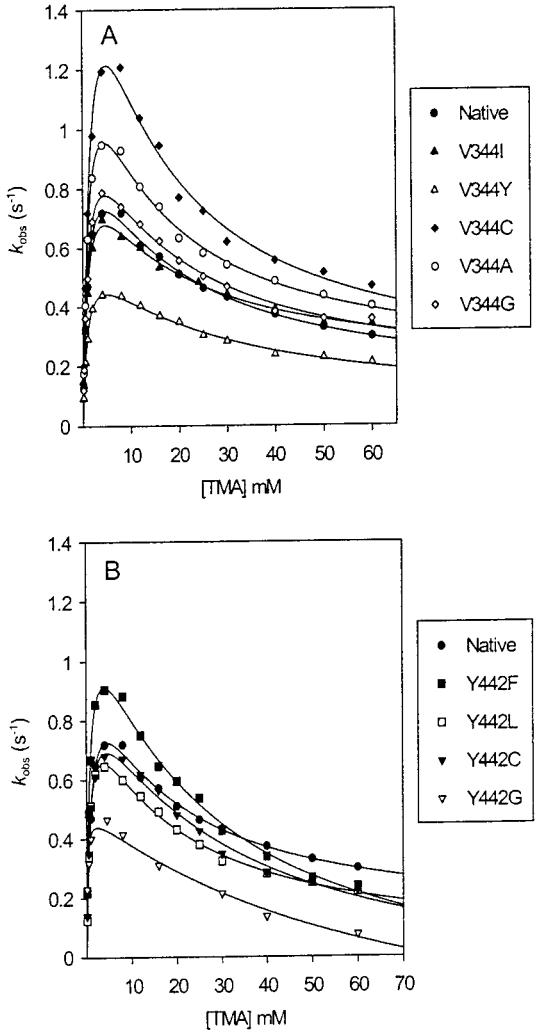

FIGURE 2: Plots of the observed rate against [TMA] for absorption changes measured at 365 nm (formation of the spin-interacting state) on mixing native and mutant TMADH enzymes with TMA. (A) Data for the native enzyme and mutants at position 344. (B) Data for the native enzyme and mutants at position 442. Reaction conditions: 50 mM potassium phosphate buffer at pH 7 and 20 °C. To aid visualization, data were fitted using eq 1. However, it is important to note (as described in ref *21*) that there is no direct correlation between the observed behavior at 365 nm seen in single-turnover studies as shown in this figure and the observed steady-state behavior in which substrate affects inhibition at high concentrations. For this reason, kinetic constants arising from fitting to eq 1 have no obvious meaning, and values are therefore not given.

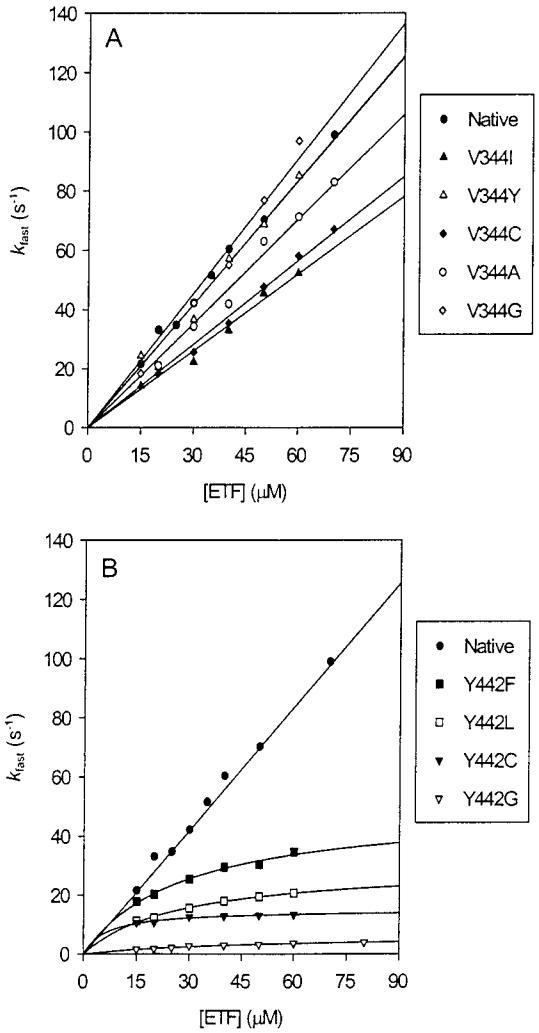

FIGURE 3: Plots of the observed rate vs [ETF] for reactions of one-electron-reduced TMADH with ETF under anaerobic conditions. (A) Data for native and V344 mutant enzymes. (B) Data for native and Y442 mutant enzymes. Reaction conditions: 50 mM potassium phosphate buffer at pH 7 and 5 °C.

series of enzymes, which again may reflect minor structural changes around the 4Fe−4S center.

Kinetics of the Oxidative Half-Reaction with ETF. The rate of electron transfer from the 4Fe−4S center of native and mutant TMADH enzymes to the flavin of ETF was measured directly using stopped-flow spectroscopy at 5 °C. The kinetics of the electron transfer reaction were simplified by using a form of TMADH in which the flavin was rendered redox inactive by treatment with phenylhydrazine (*6*, *24*, *25*). Subsequent reduction of the 4Fe−4S center of this enzyme under anaerobic conditions with sodium dithionite, followed by rapid mixing of the one-electron-reduced enzyme with ETF, enabled electron transfer to ETF to be followed without complications arising from internal electron transfer in TMADH. Measurements were taken at 5 °C, and not at 25 °C as previously done with the native enzyme (*24*), thereby slowing the rate of electron transfer and facilitating more accurate analysis of the biphasic transients when using ETF as the redox acceptor (Figure 3).

Previous studies with native TMADH have suggested that the rate of electron transfer from the 4Fe−4S center of TMADH to the flavin of ETF displays a hyperbolic dependence on ETF concentration (*24*, *27*). As discussed previously, the kinetic transients observed with ETF are complex, but they approximate biphasic behavior (*24*).[3] The experiments conducted in this paper were performed in an anaerobic glovebox, making the technical challenges associated with the analysis of electron transfer in this system much less demanding. In this work, we have analyzed the rate of electron transfer to ETF using several different preparations of oxidized ETF (prepared freshly since ETF in the oxidized form is labile). Additionally and importantly, a split time base function was applied during data acquisition to ensure

[3] The complex nature of the kinetic transients may in part be due to the highly dynamic nature of ETF, which is known to populate different conformations (*14*). It is unlikely, therefore, that in stopped-flow experiments a single conformation of ETF reacts with TMADH, an assumption that is implied in the kinetic analysis.

Table 4: Kinetic Data for the Reaction of One-Electron-Reduced, Phenylated TMADH with Oxidized ETF[a]

	reactions with ETF			reactions with Fc^+
enzyme	k ($\times 10^6$ M^{-1} s^{-1})	k_{lim} (s^{-1})	K_d (μM)	k ($\times 10^6$ M^{-1} s^{-1})
native TMADH	1.44 ± 0.02	na[b]	na	4.24 ± 0.13
V344A	1.18 ± 0.03	na	na	6.11 ± 0.03
V344C	0.94 ± 0.02	na	na	8.19 ± 0.2
V344G	1.52 ± 0.05	na	na	15.3 ± 0.27
V344I	0.87 ± 0.03	na	na	0.24 ± 0.003
V344Y	1.4 ± 0.04	na	na	0.4 ± 0.004
Y442F	1.76 ± 0.33[c]	49.6 ± 2.9	28.3 ± 3.8	2.18 ± 0.02
Y442L	1.18 ± 0.12[c]	29.0 ± 0.9	24.6 ± 1.9	1.19 ± 0.03
Y442C	2.25 ± 0.45[c]	14.9 ± 0.5	$6.6. \pm 1.1$	2.46 ± 0.06
Y442G	0.14 ± 0.03[c]	6.3 ± 0.5	45.9 ± 6.5	2.23 ± 0.03

[a] Reaction conditions: 50 mM potassium phosphate buffer at pH 7 and 5 °C. [b] na, not applicable. [c] Calculated as k_{lim}/K_d. Ferricenium data at 25 °C.

that a maximum number of data points (1000) were acquired during the fast phase alone. Also, we have included more points on the plot of the reaction rate versus ETF concentration and taken the ETF concentration to higher values than has been done previously. Under the conditions reported in this paper, in all cases, we observe very similar kinetic behavior with different preparations of ETF. These differences in experimental design likely explain the different kinetic behavior for the native enzyme observed in this paper and that reported previously (*24*, *27*). Thus, in contrast with previous reports, with the native enzyme, the rate of electron transfer to ETF was found to increase linearly as a function of ETF concentration (Figure 3) with a second-order rate constant of 1.44×10^6 M^{-1} s^{-1} for electron transfer. Similar linear dependencies on ETF concentration were observed with all the mutants altered at position 344. The second-order rate constants for these mutants are on the order of 1×10^6 to 2×10^6 M^{-1} s^{-1} (Table 4), suggesting that Val-344 does not play a major role in electron transfer to ETF (Figure 3A).

In contrast to the mutants altered at position 344 and the native enzyme, mutants altered at position 442 displayed a hyperbolic dependence on the ETF concentration (Figure 3B). Saturation behavior with respect to ETF concentration has also been observed in our previous studies of the Y442F, Y442L, and Y442G TMADH mutants (*27*). Values for k_{lim} (the limiting rate constant for electron transfer to ETF) and K_d (dissociation constant for the TMADH−ETF complex), obtained from fits of the data to a standard hyperbolic expression, were used to calculate the second-order rate constant k_{lim}/K_d (Table 4). This facilitated direct comparison with the native data (Table 4). With these mutants the TMADH−ETF complex, dissociation constants were in the range of 6−46 μM and k_{lim} values varied from 6 (Y442G) to 50 s^{-1} (Y442F). In the low-ETF concentration regime, the Y442F and Y442L mutants have second-order rate constants that are similar to the native enzyme, whereas that for the Y442C mutant TMADH is slightly increased in comparison to that of the native, due mainly to a lower apparent dissociation constant for the TMADH−ETF complex. In the Y442G mutant, an increase in the apparent dissociation constant for the complex, together with a reduction in the rate of electron transfer to ETF, results in a more than 10-fold decrease in the second-order rate constant compared with that of the native enzyme.

Kinetics of the Oxidative Half-Reaction with Fc^+. We demonstrated previously that reactions of three-electron-reduced TMADH (generated by titration with sodium dithionite) with Fc^+ give rise to transients that were fitted satisfactorily using a double-exponential expression (*32*). The two kinetic phases are well-resolved, and we have shown (on the basis of amplitude analysis with the native and Y442G mutant enzyme) that the faster phase represents electron transfer from the 4Fe−4S center to Fc^+. The slower phase represents the transfer of the remaining two electrons from the flavin of TMADH to Fc^+ via the 4Fe−4S center (*32*). Given the ease by which these transients are analyzed, compared with the difficulties associated with the analysis of transients when ETF is used as the electron acceptor (see above), we elected to study electron transfer without prior modification of TMADH with phenylhydrazine. Additionally, it was not necessary to reduce the temperature to 5 °C to obtain good quality transients. As before, a split time base was used to maximize the number of data points in the fast phase of the transient.

For the native enzyme, as with all the mutants that were studied, plots of k_{fast} versus Fc^+ concentration were linear (Figure 4); the second-order rate constants from these plots are given in Table 4. Mutation of Val-344 in TMADH has quite different effects on the rate of electron transfer to Fc^+, depending on the nature of the substitution. The smaller amino acid substitutions of Cys, Ala, and Gly all lead to an *increase* in the second-order rate constant for Fc^+ reduction (nearly 4-fold in the case of the V344G mutant). In contrast, the bulkier side chains of Ile and Tyr lead to a decrease in the value of the second-order rate constant (nearly 20-fold for V344I TMADH) when compared to that of the native enzyme. These results indicate that Val-344 is an important residue for electronic coupling to Fc^+. The data suggest that faster rates are achieved by reducing the pathway length (i.e., by shortening the length of the side chain at position 344), whereas slower transfer rates are the result of increasing pathway length (by increasing the size of the side chain). Similar kinetic investigations with the mutants altered at position 442 revealed a lack of major sensitivity in the value for the second-order rate constant (approximate range from 1×10^6 to 2×10^6 M^{-1} s^{-1}) as a function of mutation (Table 4 and Figure 4). These data therefore suggest that coupling to the Fc^+ ion does not predominantly take place through Tyr-442 in the native enzyme, although modification at this site may influence the geometry of the interaction of the Fc^+ ion with Val-344.

The program ET_Rates relates the intrinsic rate of electron transfer (k_{eT}) for exergonic tunneling (eq 2) to the edge-to-

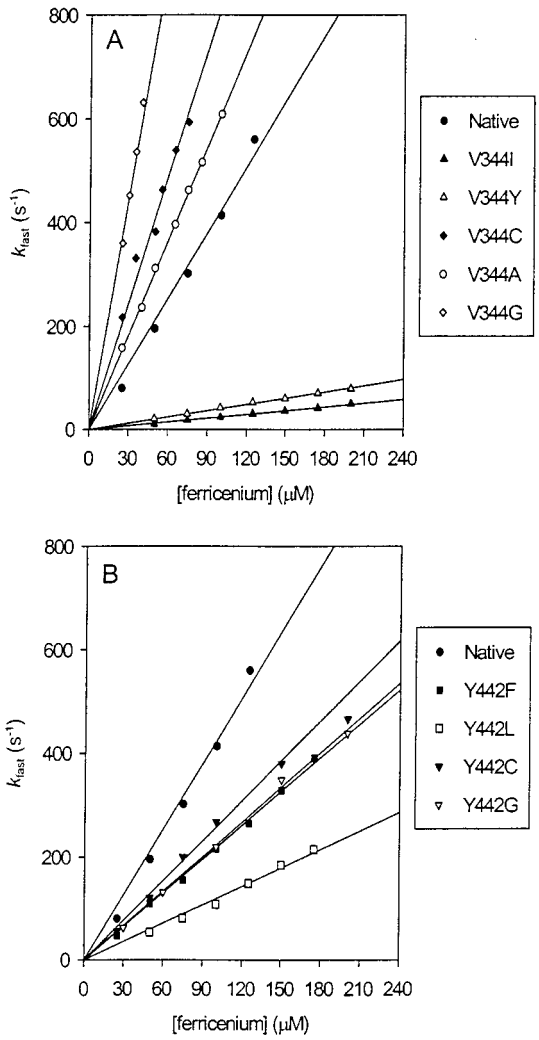

FIGURE 4: Plots of the observed rate vs [Fc^+] for reactions of three-electron-reduced TMADH with Fc^+ under anaerobic conditions. (A) Data for native and V344 mutant enzymes. (B) Data for native and Y442 mutant enzymes. Reaction conditions: 50 mM potassium phosphate buffer at pH 7 and 25 °C.

edge transfer distance (R), packing density (ρ) of protein atoms in the volume between redox centers (to account for variation in the electronic decay factor β), the driving force ΔG, and the reorganization energy λ. This empirical approach to calculating intrinsic rates of electron transfer is distinct from the approach used by the Pathways II algorithm (*38*), which explicitly recognizes protein structural heterogeneity in defining well-bonded pathways between donor and acceptor redox centers. We used the latter algorithm to identify potential major electron transfer pathways to the surface of TMADH as a prelude to mutagenesis studies. Although the Pathways II algorithm has been used extensively to visualize potential electron transfer pathways in proteins, the underlying premise (maximized electronic coupling having evolved by well-bonded pathways) has been questioned (*36*). Moreover, the Pathways II approach, although qualitatively useful in visualizing potential pathways, does not allow the intrinsic electron transfer rates to be calculated. To calculate the intrinsic electron transfer rates in native and mutant TMADH enzymes, the highest-ranked Fc^+ docking was used (these are shown pictorially in Figure 6B−K). Since this was closely similar to the other nine highest-ranking dockings, the use of only this single model of each complex in the calculation of k_{eT} is justified. The calculated electron transfer rates are given in Table 5, and these have been compared with the experimentally observed rates of electron transfer (Table 4). Clearly, a direct comparison between experimental (second-order) and calculated (first-order) electron transfer rates is not possible. However, the trends with respect to native TMADH can be compared since any perturbation in the intrinsic rate may manifest itself as a change in the observed rate. This comparison is given in the latter two columns of Table 5.

DISCUSSION

Electron Transfer to ETF and Fc^+. Our previous modeling studies of the electron transfer complex formed between TMADH and ETF have indicated that a large-scale structural reorganization of ETF most likely accompanies complex formation (*12*). This large-scale structural change is facilitated by two hinge regions in the ETF molecule linking domain II to domain I and domain II to domain III. Evidence for these predicted conformational changes has recently been obtained from UV−visible spectrophotometric and redox studies of ETF in complex with TMADH (*11*), and also from small-angle X-ray diffraction studies of oxidized and reduced (semiquinone) ETF (*14*). In free solution, ETF populates many conformations, with domain II pivoting about two hinge regions with respect to domains I and III. In forming a transient complex with TMADH, this domain motion is "frozen" and the "open", eT-active conformation of ETF is positioned on the surface of TMADH, such that the flavin is presented close to the surface groove close to residues Val-344 and Tyr-442 (*12*). This finding is consistent with the results of mutagenesis experiments reported previously (*27*) and in this paper. Val-344 of TMADH is the closest surface residue to the 4Fe−4S center, and since it is in van der Waals contact with Cys-345 (a cysteinyl ligand of the 4Fe−4S center), it is predicted to be a "hot spot" for electron transfer out of the enzyme. Our data for mutants altered at this position indicate that Val-344 is indeed a hot spot for electron transfer to Fc^+, but that coupling to ETF is only moderately affected by these mutations.

Our studies with mutants altered at residue Tyr-442 indicate that electron transfer to Fc^+ is not affected significantly. However, electron transfer to ETF is dramatically perturbed (especially for the Gly-442 mutant), indicating that this position is more important for electron transfer to ETF than Val-344. We conclude that the isoalloxazine ring is unable to extend to Val-344 at the bottom of the groove on the surface of TMADH in the productive electron transfer complex, and that electron transfer is thus via the longer route involving a pathway that exits the protein at Tyr-442. The reduced electron transfer rates with mutant enzymes altered at position 442 can be rationalized in terms of a longer electron transfer pathway and/or changes in packing density as a result of small geometrical realignments of ETF and TMADH in the productive electron transfer complex.

The appearance of saturation kinetic behavior in the mutants at position 442 deserves further comment, especially in light of the fact that complex formation ($K_d \sim 10$ μM) can be seen under *equilibrium* conditions in analytical ultracentrifugation experiments (*26*) and spectroscopic titra-

Table 5: Calculated Intrinsic Rates of Electron Transfer from the 4Fe−4S Center of TMADH to Fc^+ and to the Center of the Fe Atom of Fc^+

enzyme	edge-to-edge distance[a] (Å)	packing density[b] (ρ)	intrinsic rate constant, k_{eT} (s^{-1})	theoretical rate relative to native	experimental rate relative to native[c]
			Calculated Rates to Fc^+ as a Whole		
native TMADH	10.0	0.81	5.1×10^8		
V344A	9.69	0.84	1.0×10^9	2.0	1.4
V344C	10.0	0.83	6.5×10^8	1.3	1.9
V344G	8.69	0.88	5.3×10^9	10	3.6
V344I	11.2	0.68	1.7×10^7	0.033	0.057
V344Y	11.1	0.75	5.2×10^7	0.10	0.094
Y442F	10.0	0.82	5.5×10^8	1.1	0.51
Y442L	10.4	0.79	2.6×10^8	0.51	0.28
Y442C	9.79	0.78	4.4×10^8	0.86	0.58
Y442G	9.84	0.76	3.5×10^8	0.69	0.53
			Calculated Rates to the Center of the Fe Atom of Fc^+		
native TMADH	11.8	0.81	5.3×10^7		
V344A	10.9	0.91	6.7×10^8	13	1.4
V344C	11.5	0.87	1.8×10^8	3.4	1.9
V344G	10.3	0.95	2.1×10^9	40	3.6
V344I	12.4	0.54	3.1×10^5	0.0058	0.057
V344Y	12.4	0.74	7.8×10^6	0.15	0.094
Y442F	11.8	0.81	5.6×10^7	1.1	0.51
Y442L	11.8	0.77	2.6×10^7	0.49	0.28
Y442C	11.2	0.69	1.9×10^7	0.36	0.58
Y442G	11.5	0.73	2.2×10^7	0.42	0.53

[a] The edge-to-edge distance refers to the "shortest" distance between the two redox centers [calculated with ET_Rates (*36*)]. [b] The packing density (ρ) refers to the packing of protein atoms in the space between redox centers. When the protein medium is fully packed, $\rho = 1$. In principle, the packing density can vary from 0 to 1 [calculated with ET_Rates (*36*)]. [c] The experimentally observed electron transfer rates are given in Table 4.

Scheme 1

$$A + B \underset{k_{-a}}{\overset{k_a}{\rightleftharpoons}} (AB) \xrightarrow{k_{eT}} (A^+B^-) \longrightarrow A^+ + B^-$$

tion experiments (*11*). The simplest kinetic model describing interprotein electron transfer is shown in Scheme 1, where A is $TMADH_{1e}$ and B is ETF_{ox}. An expression for the first-order rate constant k_{obs} measured in stopped-flow experiments can be derived, with the assumption that the rate of formation of the TMADH−ETF complex equals its rate of decay [i.e., the steady-state assumption applies (*39*)]:

$$k_{obs} = \frac{k_a k_{eT}[A]}{k_{-a} + k_{eT} + k_a[A]} \quad (3)$$

The expression is hyperbolic when k_{obs} is plotted against [A]. However, when $k_{eT} \gg k_{-a} + k_a[A]$, then $k_{obs} = k_a[A]$; i.e., the reaction rate is proportional to [A]. This is the "diffusion-limited" regime where the rate of reaction cannot be faster than the rate at which TMADH and ETF form a productive electron transfer complex. The kinetic model depicted in Scheme 1 is likely to be an oversimplification for the TMADH and ETF system, since it is known that ETF undergoes a large structural change (with an associated rate constant for this process). Given the highly dynamic nature of ETF, it is likely that following the initial collision with TMADH, ETF needs to be "locked in" to the electron transfer complex, requiring additional small-scale conformational changes. Unequivocal evidence for conformational intermediates following the formation of an initial encounter complex remains to be obtained, but given the dynamic nature of the TMADH−ETF interaction, one needs to acknowledge the likely existence of such intermediates in modeling the kinetics of the oxidative half-reaction. A more realistic kinetic model, therefore, would recognize the existence of an

Scheme 2

$$A + B \underset{k_{-a}}{\overset{k_a}{\rightleftharpoons}} (AB)_1 \underset{k_{-r}}{\overset{k_r}{\rightleftharpoons}} (AB)_2 \xrightarrow{k_{eT}} (A^+B^-) \longrightarrow A^+ + B^-$$

intermediate that forms prior to the formation of the productive electron transfer complex as shown in Scheme 2. An analytical rate equation can be derived for such a scheme (eq 4):

$$k_{obs} = \frac{k_a k_r k_{eT}[A]}{k_{-a}(k_{eT} + k_{-r}) + k_r k_{eT} + k_a(k_{eT} + k_r + k_{-r})[A]} \quad (4)$$

In the regime where $k_{eT} \gg k_r \sim k_{-r}$, eq 4 reverts to eq 3, except that k_{eT} becomes k_r. Alternatively, when $k_r \gg k_{-r} > k_{-eT}$, eq 4 also reverts to eq 3, except that K_a (i.e., k_a/k_{-a}) in eq 3 has now to be interpreted as $K_a K_R$ (K_R being the equilibrium constant for conformational realignment in the complex). Thus, in the regime where the *intrinsic* electron transfer rate (k_{eT}) is fast, and also where $k_r \gg k_{-a} + k_a[A]$, eq 4 can be approximated to a linear relationship between k_{obs} and [A]. These deliberations serve to illustrate that kinetic behavior similar to that seen in the simplified model (Scheme 1) can also arise in the more complex situation (Scheme 2).

The native and Val-344 mutants with ETF as the electron acceptor do not display saturation kinetic behavior, implying that complex formation is rate-limiting, and that the intrinsic rate of electron transfer (and any conformational reorganization in the complex) following complex formation is fast. The appearance of saturation kinetic behavior for mutants altered at residue Tyr-442 could be the result of a reduction in the value of the intrinsic electron transfer rate constant (k_{eT}). However, perhaps more likely (given the relatively slow observed limiting rates of electron transfer for the Tyr-442 mutant TMADH enzymes) is a reduction in the rate constant

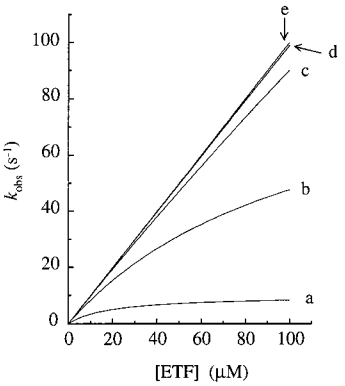

FIGURE 5: Simulation of observed electron transfer rates as a function of [ETF]. Simulations were performed using eq 3. Values of k_a and k_{-a} were fixed at 1×10^6 M^{-1} s^{-1} and 10 s^{-1}, respectively, corresponding to the measured equilibrium dissociation constant (K_d) for the electron transfer complex of ~10 μM. Simulations were performed over a range of values for the intrinsic rate of electron transfer (k_{eT}): (a) $k_{eT} = 10^1$ s^{-1}, (b) $k_{eT} = 10^2$ s^{-1}, (c) $k_{eT} = 10^3$ s^{-1}, (d) $k_{eT} = 10^4$ s^{-1}, and (e) $k_{eT} = 10^5$ s^{-1}. For a k_{eT} of $>10^6$ s^{-1}, curves are superimposed on curve e.

describing reorganization of a precomplex in forming the productive electron transfer complex. In either scenario, this leads to the predicted hyperbolic relationship between k_{obs} and [A]. To illustrate this aspect, we have performed simulations of the observed rate of electron transfer as a function of [ETF] using eq 3 (Figure 5). In this simulation, k_a was fixed at 1×10^6 M^{-1} s^{-1} (not an unrealistic value for the encounter kinetics of two protein molecules in solution). The known dissociation constant for the electron transfer complex measured under equilibrium conditions is ~10 μM, thus fixing k_{-a} at 10 s^{-1}. Our simulations are for k_{eT} ranging from 10^1 to 10^9 s^{-1}. These simulations clearly reveal that for values of k_{eT} in excess of 10^3 s^{-1} there is essentially a linear relationship between k_{obs} and [ETF] (curves c−e in Figure 5). When k_{eT} is less than 10^3 s^{-1}, the simulations reveal a hyperbolic dependence of k_{obs} on [ETF] (curves a and b in Figure 5). The values for k_{obs} arising from the simulation are very similar to the experimentally determined values for the native and Y442 mutant TMADH enzymes (Figure 3B). Hyperbolic dependence only occurs when k_{eT} is less than ~10^3 s^{-1}. These values for k_{eT} are in all likelihood too low to correspond to intrinsic electron transfer rate constants in the Y442 TMADH mutant enzymes for transfers occurring over a distance of about 11−12 Å (*36*). Rate limitation in this kinetic regime is most likely the result of impaired structural reorganization in the electron transfer complex (Scheme 2), and rate constants of this magnitude (10^1−10^3 s^{-1}) are consistent with large dynamical changes in proteins. As discussed above, eq 4 (which describes Scheme 2) reduces to eq 3 when $k_{eT} \gg k_r$ or ~k_{-r} except that k_{eT} becomes k_r. Our simulations are therefore equally valid for the more complex scheme (Scheme 2) which invokes structural reorganization during electron transfer complex assembly. Attempts to measure the rates of conformational change occurring during electron transfer complex formation are technically challenging and are currently being investigated, and these results should throw more light on to the complexities of this interprotein electron transfer reaction. A possibility is that the phenolic hydroxy group of Tyr-442 makes a direct interaction with ETF and may thus contribute to enhanced rates of reorganization in the native electron transfer complex. Clearly, the mechanism of electron transfer in the TMADH−ETF complex cannot be modeled as a simple two-step "collision plus transfer" process (i.e., Scheme 1), and further work is needed to provide a detailed kinetic and structural description of this electron transfer reaction.

Computational analysis of the intrinsic rate of electron transfer to ETF is difficult, given the lack of structural information for the complex formed between TMADH and ETF. However, analysis with Fc^+ is more tractable, due to the small size of the Fc^+ cation. Docking analysis suggests that Fc^+ binds in a similar (but not identical) location in the native and mutant TMADH enzymes (Figure 6B−K). In the optimally docked conformations, the intrinsic electron trans-

Scheme 3

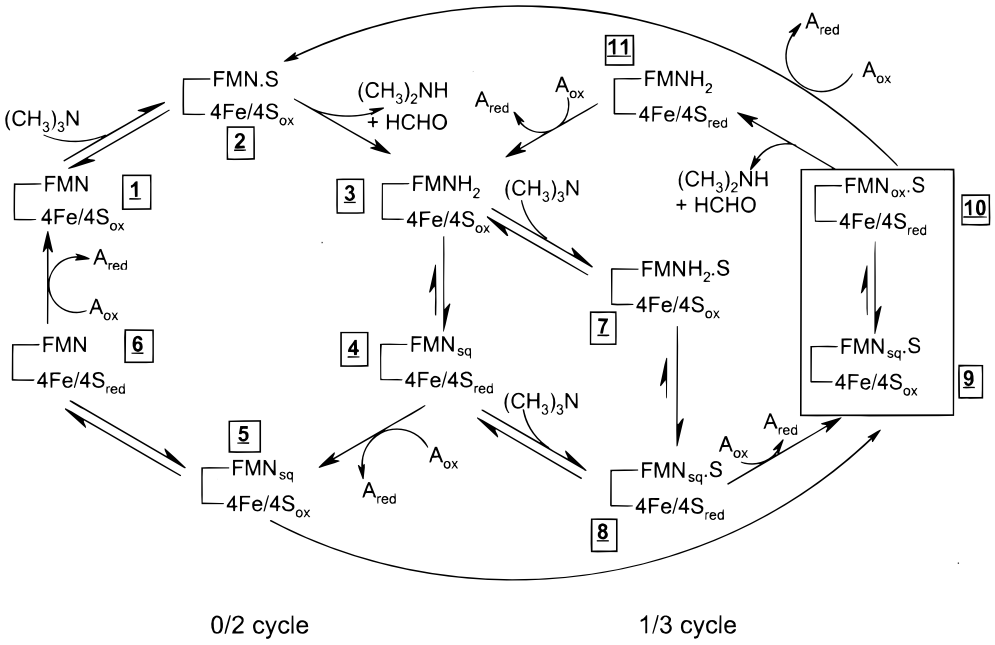

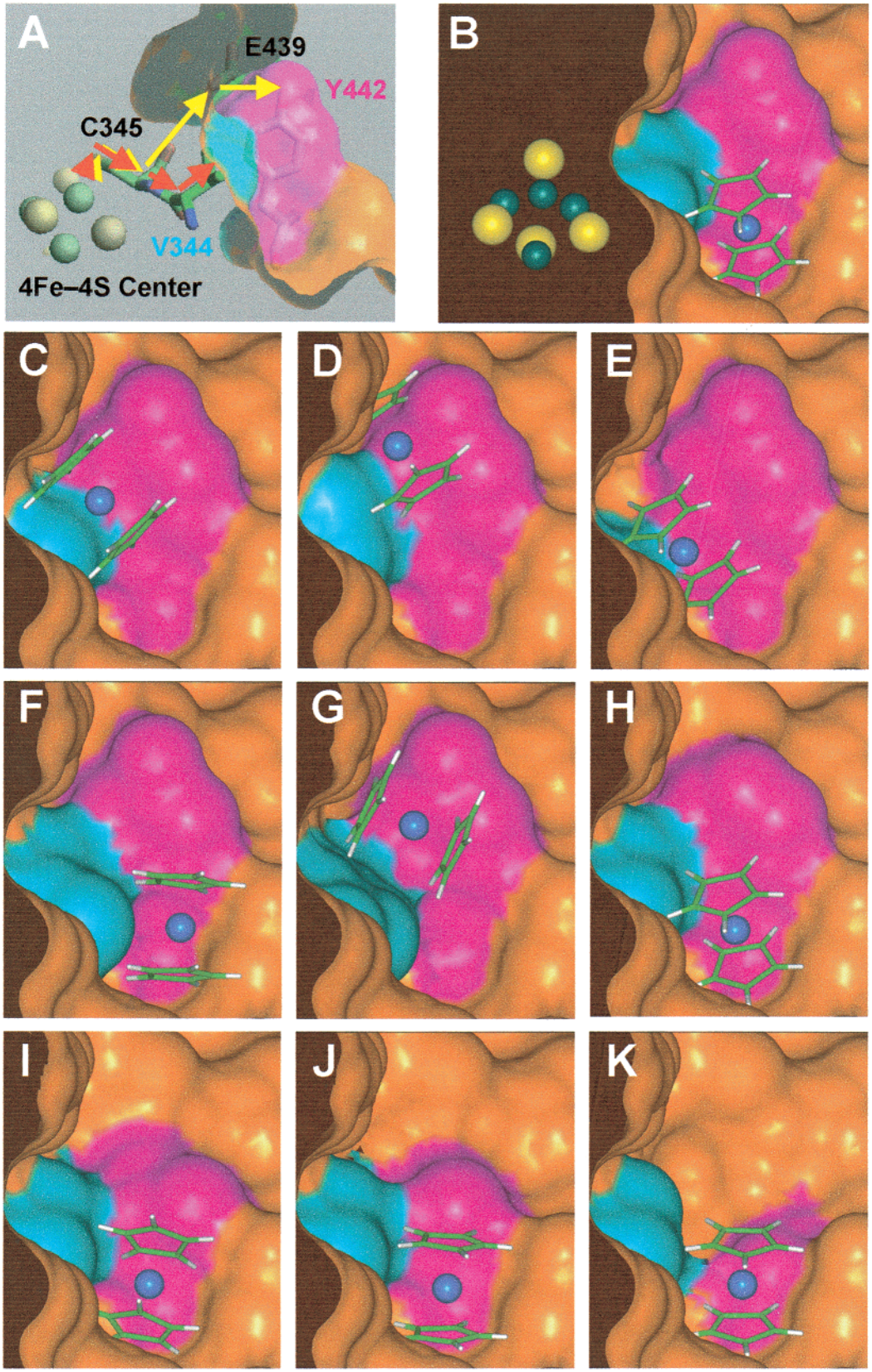

FIGURE 6: Molecular graphics representation of the surface topology of TMADH showing the groove and the positions of residues 344 (cyan) and 442 (magenta). (A) The two major predicted "through-bond" electron transfer pathways from the 4Fe−4S center to the surface of the enzyme are indicated in red (via V344) and yellow (via Y442). (B) How Fc^+ is able to penetrate the surface groove of native TMADH. For clarity, the view has been rotated slightly with respect to that in panel A. Panels C−K are the same orientation as panel B (but with the 4Fe−4S center not shown) and show the position of Fc^+ in (C) V344A, (D) V344C, (E) V344G, (F) V344I, (G) V344Y, (H) Y442F, (I) Y442L, (J) Y442C, and (K) Y442G. This figure should be considered in conjunction with Table 5.

fer rate constant calculated using the program ET_Rates is sensitive to the approach used. Electron transfer from the 4Fe−4S center to Fc^+ as a whole (Table 5) gives a k_{eT} in the range of 10^7−10^9 s^{-1}. Generally, this reflects the

experimental observations that electron transfer to Fc^+ is a function of the residue at position 344, but is independent of the residue at position 442 (Table 5). The correlation between calculated and experimental results is not as good if the intrinsic rate constants are calculated instead between the 4Fe−4S center and the Fe atom of Fc^+ (Table 5). Considering mutations of V344, the smaller side chains (V344A, V344C, and V344G) were correctly predicted to have enhanced electron transfer rates compared with that of native TMADH. This is likely due to a shorter electron transfer pathway, and/or an increased packing density, from the 4Fe−4S center to Fc^+, because the Fc^+ can lie closer to the backbone of residue 344 (Table 5 and Figure 6B−E). Also, the larger side chains at position 344 (V344I and V344Y) were correctly predicted to have reduced electron transfer rates compared with that of native TMADH. The Fc^+ is prevented from approaching as closely to the protein backbone; this is reflected in the increased edge-to-edge distance and the reduced packing density (Table 5 and Figure 6B,F,G). Interestingly, mutations at position 442 did not affect by more than a factor of 2 the intrinsic rate constant, regardless of side chain size, and the docking analysis suggests that mutating the residue at position 442 has little effect on the location at which the Fc^+ binds (Table 5 and Figure 6B,H−K). This is consistent with experimental observations of coupling through position 344 (and not position 442) to Fc^+. Furthermore, in almost all cases, the Fc^+ docks between positions 344 and 442, yet only position 344 was found to be sensitive to the electron transfer mechanism. This implies that electron transfer is via the shortest route from the 4Fe−4S center to Fc^+ involving residue 344, but not residue 442. The poorer correlation between experimental and calculated rates for electron transfer to the iron in Fc^+, rather than the Fc^+ as a whole, raises an interesting point. It is consistent with the common dogma that there is no resistance ($\beta = 0$; i.e., there is no decay in the electronic wave function) in Fc^+.

Steady-State Behavior and Effects of Modulating the Electron Transfer Rate. Our studies have revealed that we can both increase and decrease the rates of electron transfer to Fc^+ by making alterations to pathway length and/or packing density through modification of the side chain volume at residue 344. Our analyses of the TMADH enzymes altered at residue Val-344 have demonstrated that this has profound effects on the steady-state kinetic behavior, which needs to be rationalized in the context of the scheme (Scheme 3) advanced for the native enzyme. Steady-state reactions with ETF exhibited a hyperbolic dependence on [ETF] for all the enzymes that were studied. For technical reasons, these experiments were restricted to a [ETF] range of 0−90 μM, due to the very high absorbance values when [ETF] > 90 μM. By contrast, the steady-state experiments with Fc^+ were conducted over a wider concentration range (0−250 μM). From stopped-flow studies, the second-order rate constant for electron transfer to Fc^+ is about 3-fold greater than that with ETF for the native enzyme, but these experiments were conducted at 25 °C (and not 5 °C as for the ETF experiments). The second-order rate constants are probably comparable when the temperature differences are taken into account. Thus, the rates of electron transfer from the 4Fe−4S center to Fc^+ under steady-state conditions are likely to be faster at the higher end of the extended [Fc^+] range than the rates measured at the higher end of the restricted [ETF] range.

As shown in Figure 1A, the rate of electron transfer to Fc^+ affects the partitioning between the 1/3 cycle and the 0/2 cycle shown in Scheme 3. At a fixed TMA concentration of 100 μM, an equilibrium is established between species **4** and species **8** and also species **3** and **7** (Scheme 3) prior to the addition of Fc^+. The equilibrium distribution of the species will be affected by the [TMA]. On the addition of Fc^+ (at high concentrations), species **8** will rapidly convert to species **9**, committing the enzyme to the 1/3 cycle (which has poor catalytic activity due to the poor rate of conversion of species **9** to **10**, the overall rate-limiting step for this cycle). At low Fc^+ concentrations, species **8** will accumulate (due to the lower rate of conversion of species **8** to **9**). The effect will be to displace the equilibrium between species **4** and **8** in favor of species **4** and thus increase the throughput in the 0/2 cycle by increasing the rate of conversion of species **4** to **5**. The observed differences in steady-state inhibition for native TMADH in reactions with Fc^+ can therefore be rationalized in the context of Scheme 3. The steady-state behavior of the mutant enzymes can also be understood by reference to this scheme. The rates of electron transfer from the 4Fe−4S center to Fc^+ are increased in the V344G, V344A, and V344C mutants. Since the electron transfer reaction is second-order, the affect is akin to increasing the [Fc^+] with the native enzyme. Thus, the concentration range in which inhibition is seen with the mutants is lowered for the V344G, V344A, and V344C mutants, reflecting partitioning into the 1/3 cycle at lower Fc^+ concentrations. The lack of inhibition seen with the V344I and V344Y mutant TMADH enzymes is a result of electron transfer from the 4Fe−4S center to Fc^+ being rate-limiting in overall catalysis. This step is common to both the 0/2 and 1/3 redox cycles. Consequently, catalysis through the 0/2 and 1/3 catalytic cycles is now comparable, and although partitioning into the 1/3 cycle will be favored at high Fc^+ concentrations, there will be no consequence for the overall rate of steady-state turnover. The steady-state behavior of TMADH mutants altered at residue Tyr-442 can also be rationalized along lines similar to those described for mutations at position Val-344. In this case, the second-order rate constant for electron transfer to Fc^+ is slightly diminished compared with that of the native enzyme, and this correlates well with less sensitivity to Fc^+ inhibition in the steady state (Figure 1B).

CONCLUSIONS

In this paper, we have demonstrated that electron transfer from the 4Fe−4S center of TMADH to external redox acceptors can follow at least two transfer pathways. Coupling to the physiological acceptor, ETF, occurs via the longer of the two pathways exiting via Tyr-442. Coupling to the artificial acceptor, Fc^+, is via a more direct pathway involving residue Val-344. Mutation of Val-344 to small side chains *increases* the rate of electron transfer to the Fc^+ ion, as a result of shortening the electron transfer pathway and/or changes in packing density. Larger residues at position 344 (Tyr and Ile) bring about a reduction in the electron transfer rate. Together, the data reveal (i) the existence of multiple pathways in TMADH and (ii) that the nature of the electron acceptor exerts control on the selection of the electron transfer pathway as a consequence of the unique

way in which the acceptor binds to the surface of TMADH. The intrinsic rate constants of various mutants relative to that of native TMADH were found to be consistent with experimental observations.

REFERENCES

1. Steenkamp, D. J., and Mallinson, J. (1976) *Biochim. Biophys. Acta 429*, 705−719.
2. Steenkamp, D. J., and Singer, T. P. (1976) *Biochem. Biophys. Res. Commun. 71*, 1289−1295.
3. Steenkamp, D. J., McIntire, W., and Kenney, W. C. (1978) *J. Biol. Chem. 253*, 2818−2824.
4. Steenkamp, D. J., Kenney, W. C., and Singer, T. P. (1978) *J. Biol. Chem. 253*, 2812−2817.
5. Hill, C. L., Steenkamp, D. J., Holm, R. H., and Singer, T. P. (1977) *Proc. Natl. Acad. Sci. U.S.A. 74*, 547−551.
6. Kasprzak, A. A., Papas, E. J., and Steenkamp, D. J. (1983) *Biochem. J. 211*, 535−541.
7. Lim, L. W., Mathews, F. S., and Steenkamp, D. J. (1988) *J. Biol. Chem. 263*, 3075−3078.
8. Steenkamp, D. J., and Gallup, M. (1978) *J. Biol. Chem. 253*, 4086−4089.
9. Duplessis, E. R., Rohlfs, R. J., Hille, R., and Thorpe, C. (1994) *Biochem. Mol. Biol. Int. 32*, 195−199.
10. Byron, C. M., Stankovich, M. T., Husain, M., and Davidson, V. L. (1989) *Biochemistry 28*, 8582−8587.
11. Jang, M.-H., Scrutton, N. S., and Hille, R. (2000) *J. Biol. Chem. 275*, 12546−12552.
12. Chohan, K. K., Scrutton, N. S., and Sutcliffe, M. J. (1998) *Protein Pept. Lett. 5*, 231−236.
13. Roberts, D. L., Frerman, F. E., and Kim, J.-J. P. (1996) *Proc. Natl. Acad. Sci. U.S.A. 93*, 14355−14360.
14. Jones, M., Basran, J., Sutcliffe, M. J., Grossmann, J. G., and Scrutton, N. S. (2000) *J. Biol. Chem. 275*, 21349−21354.
15. Steenkamp, D. J., Singer, T. P., and Beinert, H. (1978) *Biochem. J. 169*, 361−369.
16. Steenkamp, D. J., Beinert, H., McIntire, W. S., and Singer, T. P. (1978) in *Mechanisms of oxidizing enzymes* (Singer, T. P., and Ondarza, R. N., Eds.) pp 127−141, Elsevier North-Holland Inc., New York.
17. Singer, T. P., Steenkamp, D. J., Kenney, W. I. C., and Beinert, H. (1980) in *Flavins and Flavoproteins* (Yagi, K., and Yamano, T., Eds.) pp 277−287, Japan Scientific Societies Press, Tokyo.
18. Steenkamp, D. J., and Beinert, H. (1982) *Biochem. J. 207*, 241−252.
19. Steenkamp, D. J., and Beinert, H. (1982) *Biochem. J. 207*, 233−239.
20. Rohlfs, R. J., and Hille, R. (1994) *J. Biol. Chem. 269*, 30869−30879.
21. Jang, M.-H., Basran, J., Scrutton, N. S., and Hille, R. (1999) *J. Biol. Chem. 274*, 13147−13154.
22. Lim, L. W., Shamala, N., Mathews, F. S., Steenkamp, D. J., Hamlin, R., and Xuong, N. H. (1986) *J. Biol. Chem. 261*, 15140−15146.
23. Basran, J., Sutcliffe, M. J., Hille, R., and Scrutton, N. S. (1999) *J. Biol. Chem. 274*, 13155−13161.
24. Huang, L., Rohlfs, R. J., and Hille, R. (1995) *J. Biol. Chem. 270*, 23958−23965.
25. Nagy, J., Kenney, W. C., and Singer, T. P. (1979) *J. Biol. Chem. 254*, 2684−2688.
26. Wilson, E. K., Scrutton, N. S., Colfen, H., Harding, S. E., Jacobsen, M. P., and Winzor, D. J. (1997) *Eur. J. Biochem. 243*, 393−399.
27. Wilson, E. K., Huang, L., Sutcliffe, M. J., Mathews, F. S., Hille, R., and Scrutton, N. S. (1997) *Biochemistry 36*, 41−48.
28. Scrutton, N. S., Packman, L. C., Mathews, F. S., Rohlfs, R. J., and Hille, R. (1994) *J. Biol. Chem. 269*, 13942−13950.
29. Wilson, E. K., Mathews, F. S., Packman, L. C., and Scrutton, N. S. (1995) *Biochemistry 34*, 2584−2591.
30. Lehman, T. C., Hale, D. E., Bhala, A., and Thorpe, C. (1990) *Anal. Biochem. 186*, 280−284.
31. Leatherbarrow, R. J. (1992) *Grafit*, Erithacus Software Ltd., Staines, U.K.
32. Roberts, P., Basran, J., Wilson, E. K., Hille, R., and Scrutton, N. S. (1999) *Biochemistry 38*, 14927−14940.
33. Craig, D. H., Moody, P. C. E., Bruce, N. C., and Scrutton, N. S. (1998) *Biochemistry 37*, 7598−7607.
34. Fletcher, D. A., McMeeking, R. F., and Parkin, D. (1996) *J. Chem. Inf. Comput. Sci. 36*, 746−749.
35. Kuntz, I. D., Blaney, J. M., Oatley, S. J., Langridge, R., and Ferrin, T. E. (1982) *J. Mol. Biol. 161*, 269−288.
36. Page, C. C., Moser, C. C., Chen, X. X., and Dutton, P. L. (1999) *Nature 402*, 47−52.
37. Roberts, D. L., Salazar, D., Fulmer, J. P., Frerman, F. E., and Kim, J.-J. P. (1999) *Biochemistry 38*, 1977−1989.
38. Regan, J. J. (1993) Pathways II, Molecular Simulations, Inc., San Diego.
39. Bendall, D. S. (1996) in *Protein electron transfer* (Bendall, D. S., Ed.) pp 43−68, Bios Scientific Publishers, Oxford, U.K.

BI0006868